Applied Catalysis B: Environmental 180 (2016) 94–105

Contents lists available at ScienceDirect

Applied Catalysis B: Environmental

journal homepage: www.elsevier.com/locate/apcatb

Largely Cu-doped $LaCo_{1-x}Cu_xO_3$ perovskites for TWC: Toward new PGM-free catalysts

A. Glisenti[a,*], M. Pacella[a], M. Guiotto[c], M.M. Natile[a,b], P. Canu[c]

[a] Dept. of Chemical Sciences - University of Padova, Via F. Marzolo, 1, 35131, Padova, Italy
[b] CNR-IENI, INSTM Via F. Marzolo, 1, 35131, Padova, Italy
[c] Dept of Industrial Engineering - University of Padova Via F. Marzolo, 9, 35131, Padova, Italy

ARTICLE INFO

Article history:
Received 11 February 2015
Received in revised form 8 June 2015
Accepted 11 June 2015
Available online 16 June 2015

Keywords:
Perovskite
NO_x reduction
Three-way catalysts
Carbon monoxide
Automotive
Exhaust gas

ABSTRACT

Doping of $LaCoO_3$ with copper to add reduction functionality in addition to the known oxidation properties has been investigated, aiming at three-way catalysis (TWC) applications. Nanoscale perovskites with nominal composition $LaCo_{1-x}Cu_xO_3$, ($x = 0$, 0.1, 0.3, and 0.5) have been synthesized by means of the citrate method. A stable perovskitic phase with rhombohedral geometry up to an unprecedented $x = 0.5$ has been obtained and characterized by BET, X-ray diffraction (XRD), Temperature Programmed Reduction (TPR), X-ray Photoelectron Spectroscopy (XPS), and Scanning Electron Microscopy (SEM). The crystallite size decreases with increasing the copper amount and also the morphology differs; moreover the surface reactivity with respect to atmospheric moisture and carbon dioxide is more evident in the sample with $x = 0.5$. Reactivity has been measured in simple NO + CO and CO + O_2 model reactions, as well as with complex mixtures approaching automotive exhaust composition, at both stoichiometric and O_2 limiting conditions. The catalysts have been characterized after reaction as well. The perovskite with the highest Cu amount, $LaCo_{0.5}Cu_{0.5}O_3$, exhibits an interesting compromise of oxidation and NO reduction functionality at interesting, low temperatures with very short contact time (GHSV = 1,000,000 h^{-1}). Still, activity for NO reduction in real mixtures requires substoichiometric O_2.

1. Introduction

Three-way catalysts (TWC) have to achieve the elimination of 3 different types of pollutants simultaneously. They have to facilitate oxidation of CO and unburned hydrocarbons (HC) and reduction of NO. NO should be selectively converted to N_2 instead of NO_2, NH_3 or N_2O, that are toxic or greenhouse-gases. At the present, TWC catalysts still contain expensive noble metals as Pt, Pd and Rh, as well as rare earth metals, most of them included in the list of critical raw materials.

Perovskites, on the other hand, are known as versatile materials which allow the incorporation of different cations in their structure. Thus, the incorporation of inexpensive and largely available, catalytically active transition metal cations can be helpful in developing low-cost active catalysts for TWC.

Most studies on perovskites are focused on the oxidation of CO and HC: among the perovskites reported in the literature, $LaCoO_3$ and $LaMnO_3$ perovskite based oxides, appear to be the more active for the complete oxidation of CO and HC. As early as 1971, $LaCoO_3$ was suggested to be a good catalyst for automobile exhaust treatment [1]. Subsequently, several researchers [2–5] continued to investigate $LaCoO_3$ for exhaust control trying to improve its activity by doping or by means of rhodium; two approaches have been considered: the deposition of Rh onto $LaCoO_3$ surface and the insertion of this element into the perovskite [6,7]. Cimino et al. [6], in particular, studied Rh–La(Mn,Co)O_3 monolithic catalysts for the combustion of methane under fuel-rich conditions. $La_{0.9}Ba_{0.1}CoO_3$ perovskite catalysts have been investigated for the control of CO and Particulate Matter (PM) emissions [8]. Supported lanthanum cobaltate was studied as vehicular exhaust cleaning catalyst in the oxidation of propylene [9].

Several factors influence oxidation capability: the amount of active oxygen species (α-oxygen), as an example and the mobility of lattice oxygen. Oxygen vacancies are directly connected with lattice oxygen mobility: the higher the number of anion defects, the higher the mobility of lattice oxygen [10]. One of the possibilities is increasing the oxygen mobility by means of an aliovalent doping in the perovskite A site. In general, A and B sites doping can induce the formation of structural defects (anionic or cationic vacancies) and of different oxidation states (in the B site) and can thus be funda-

* Corresponding author. Fax: +39 49 8275161.
E-mail address: antonella.glisenti@unipd.it (A. Glisenti).

http://dx.doi.org/10.1016/j.apcatb.2015.06.017
0926-3373/

mental for the catalytic activity. Also the presence of cations redox couples is determinant.

Taking into consideration these aspects, several perovskites with rather complex compositions have been investigated, showing promising activity for CO and HC oxidation. In perovskites with *B* = Co, Cr, V, Mn, Ni, Al, as an example, the influence of B cations on the structure and activity was investigated. In particular it was observed that deformation of the octahedral coordination is evident in the less active perovskites; moreover the more active catalysts are capable of extensive oxygen adsorption [11]. Another important option is doping. The partial substitution of Co with Cu in the B site, as an example, was observed to strongly influence catalyst reducibility and catalytic activity [3]; also the doping in A-site, that can increase the vacancies and affect the oxidation state of the B cations, can be effective to increase the reactivity [12–16]. Beside composition other properties can affect the catalytic activity, such as surface area [17].

On the other hand, the efficiency of perovskites in NO_x reduction is often rather poor and needs further investigations. NO_x can be converted into innocuous gases mainly by three approaches: direct decomposition, selective catalytic reduction or NO_x storage and reduction.

Although, NO_x is thermodynamically unstable and it can decompose to N_2 and O_2, which is the simplest approach to NO_x removal, the decomposition reaction is inhibited by the high activation energy (364 kJ/mol). Therefore, a catalyst is required to facilitate the reaction.

Focussing on the reaction mechanism [18] the perovskite has to be able to promote CO oxidation (and thus the oxygen mobility/exchange) and the dissociative interaction of NO. In addition, the oxygen exchange between these species is likely to happen with the intervention of the surface anion vacancies. Several perovskites have been designed in order to present these properties. Literature data suggest that good activities can be obtained considering Fe, Co, and Mn in the B site [19–21]. For NO reduction significant improvement can be obtained by means of doping in the A-site [22–24]. Another interesting possibility is synthesizing composites in which the catalytic activity can be improved by the addition of several species; as an example, the presence of Co_3O_4 significantly modifies the activity of $LaCoO_3$ [25]. However this is not a general consideration and the influence of the presence of several phases has to be investigated case by case, as confirmed by Belessi et al. [26] that focussed on the influence of Fe_2O_3 addition to the $La_{1-x}FeO_3$ perovskite, in the NO + CO reaction. In spite of the work carried out so far, we believe that perovskites really active in TWC reactions are still lacking.

Copper doped perovskites of the type $LaCo_{1-x}Cu_xO_3$ are reported to be promising oxidation catalysts in spite of the difficulties in their synthesis. Porta et al. [27] concluded that the presence of a single perovskite phase of $LaCo_{1-x}Cu_xO_3$ was solely obtained at relatively high calcination temperature (≥800 °C) with $x < 0.4$. At higher concentration of copper ($x \geq 0.4$), a $LaCu_2O_4$ phase appears in addition to the $LaCo_{1-x}Cu_xO_3$ perovskite. Tien-Thao et al. [28] investigated $LaCo_{1-x}Cu_xO_3$ perovskites ($0 \leq x \leq 0.6$) obtained by reactive grinding from the corresponding oxides. In all cases residual oxide impurities are observed in addition to the rhombohedral phase. Lower copper contents ($x \leq 0.2, 0.3$) are more usual [29–34]; in spite of the rather low amount of copper, however, the presence of minor phases (Co_3O_4, CuO) was almost always observed.

Tien-Thao et al. suggested an interesting use of $LaCo_{1-x}Cu_xO_{3-\delta}$ powders for higher alcohol synthesis [28] whereas Lisi et al. [35] focused on the redox properties and reactivity in methane catalytic combustion and Glisenti et al. [36] on the reactivity in steam reforming and oxidative steam reforming of methanol and ethanol.

Focusing on the TWC application, Zhang et al. [31] studied Cu doped $LaCoO_3$ up to $x = 0.2$, demonstrating that this perovskite was more active in the NO decomposition; the perovskites were obtained by reactive grinding, at ambient temperature. To the best of our knowledge no attempt has been done so far to investigate the reactivity of Cu-rich $LaCo_{1-x}Cu_xO_3$ perovskites.

In this work we prepared and investigated the activity in TWC reactions of $LaCo_{1-x}Cu_xO_3$ perovskites, extending the amount of Cu above earlier synthesis usually reported in the Literature, i.e. $0 \leq x \leq 0.5$. The results are correlated to the XRD (X-ray Diffraction), XPS (X-ray Photoelectron Spectroscopy), TPR (Temperature Programmed Reduction), SEM (Scanning Electron Microscopy), BET characterizations, in order to understand the role played by copper and cobalt. To gain some understanding of the reaction mechanism, we first tested the prepared catalysts in CO + NO and CO + $1/2O_2$ model reactions. In addition, we also tested the TWC activity with complex mixtures simulating an automotive exhaust, that include steam, CO_2 and hydrocarbons. Actual exhaust composition and temperature could be very different with respect to common laboratory conditions (e.g. large NO and CO concentrations, lack of O_2) and extremely challenging to prove the effective activity of the prepared samples, in order to evaluate the effective applicability of such catalytic materials.

2. Experimental

2.1. Synthesis

The samples were prepared by the citrate method starting from La_2O_3 (Aldrich 99.9%), CuO (Strem Chemicals 99.999%) and CoO (Acros 99%). Citric acid monohydrate (Sigma–Aldrich 99%) is added to an aqueous solution of the cations (obtained by mineralization with nitric acid of the corresponding precursors) with a molar ratio of 1.9:1 with respect to the total amount of cations. Then the solution is heated up to 80 °C to promote water evaporation and to obtain a wet-gel. The gel is heated to 400 °C for 2 h in air to decompose the organic framework.

At the end of the heat treatment, the powder is grinded and calcined at 600 °C, for 6 h. The same procedure was adopted for the synthesis of $LaCoO_3$; in this case the powder was calcined at 650 °C (the minimum temperature to obtain the pure perovskitic phase).

2.2. Characterization

The XPS measurements were carried out with a PerkinElmer Φ 5600 ci Multi Technique System. The spectrometer was calibrated by assuming the binding energy (BE) of the Au $4f_{7/2}$ line to be 84.0 eV with respect to the Fermi level. Both extended spectra (survey −187.85 eV pass energy, 0.5 eV·step^{-1}, 0.05 s·step^{-1}) and detailed spectra (for La 3d, Cu 2p, Co 2p, O 1 s and C 1 s −23.50 eV pass energy, 0.1 eV·step^{-1}, 0.1 s·step^{-1}) were collected with a standard Al Kα source working at 300 W. The standard deviation in the BE values of the XPS line is 0.10 eV. The atomic percentage, after a Shirley-type background subtraction [37], was evaluated by using the PHI sensitivity factors [38]. The peak positions were corrected for the charging effects by considering the C 1 s peak at 285.0 eV and evaluating the BE differences [39].

The XRD analyses were performed with a Bruker D8 Advance diffractometer with Bragg–Brentano geometry using a Cu Kα radiation (40 kV, 40 mA, λ = 0.154 nm). The data were collected at 0.03° at a counting time of 10 s/step in the (2θ) range from 10° to 90°. The crystalline phases were identified by the search-match method using the JCPDS database. The phase compositions, structure, lattice parameters, and crystallite sizes of the powders were determined by Rietveld powder structure refinement analysis of XRD data, by using the MAUD (Material Analysis Using Diffraction) software [40], applying the RITA/RISTA method as developed by

Table 1
Feed composition of the second set of catalytic tests($\Lambda = O_2$ fed/O_2 stoich).

He	CO_2	H_2O	O_2	CO	NO	H_2	CH_4	C_3H_6	C_3H_8	Λ	
Balance	15%	10%	0.777%	0.700%	0.100%	0.233%	0.023%	0.045%	0.023%	1.0	Stoich
Balance	15%	10%	0.609%	0.900%	0.100%	0.300%	0.030%	0.060%	0.030%	0.6	Rich

Table 2
Specific surface area by BET; structure, lattice parameters, and crystallite sizes calculated by Rietveld method[a] of $LaCo_{1-x}Cu_xO_3$ samples after calcination at 650 ($LaCoO_3$) and 600 °C ($LaCo_{1-x}Cu_xO_3$).

Sample	Specific surface area (m^2/g)	Crystallite size (nm)	Cell parameters[a] (Å) α(°)		Perovskite structure
$LaCoO_3$	10	42(2)	5.385(0.001)	60.67(0.01)	Rhombohedral
$LaCo_{0.9}Cu_{0.1}O_3$	14	47(5)	5.391(0.001)	60.74(0.01)	Rhombohedral
$LaCo_{0.7}Cu_{0.3}O_3$	14	39(8)	5.406(<0.001)	60.69(0.01)	Rhombohedral
$LaCo_{0.5}Cu_{0.5}O_3$	17	26(2)	5.424(0.01)	60.63(0.01	Rhombohedral

[a] The error values are reported in parentheses.

Wenk et al. [41] and Ferrari and Lutterotti [42]. The Rietveld method has given a reasonable fit of the diffraction profiles (Rwp ≤ 5%). The required crystallographic data were taken from ICSD (Inorganic Crystal Structure Database, version 2007, Fachinformationszentrum, Karlsruhe, Germany).

Temperature Programmed Reduction (TPR) and BET specific surface area measurements were performed with an Autochem II 2920 Micromeritics, equipped with a TCD detector. The TPR measurements were carried out in a quartz reactor by using 50 mg of sample and heating from RT to 900 °C at 10 °C min^{-1} under a constant flow of H_2 5% in Ar (50 ml min^{-1}). TPR samples were previously outgased with He (50 ml min^{-1}) at RT. In BET measurements 100 mg of sample were used; before measurement the sample was treated at 350 °C under a constant flow of He (50 ml min^{-1}); each surface area value is the result of three consecutive measurements.

The IR spectra were collected with a Bruker Tensor 27 spectrometer (accumulating 32 scans at a resolution of 1 cm^{-1}) in a flow chamber for gas analysis, fitted with NaCl windows. The spectrum of the chamber in argon flow was used as background.

2.3. Catalytic tests

Two series of activity tests were carried out. The first set of measurements used simplified mixtures to investigate the mechanism. 40 mg of sample were loaded in a glass reactor of 6 mm internal diameter; the temperature was monitored by a thermocouple inserted right upstream of the bed. In this configuration we studied the NO + CO reaction, using a stoichiometric mixture containing 4% CO and 4% NO, a total flow rate of 100 ml/min and atmospheric pressure. The CO + O_2 reaction was studied using stoichiometric amounts of reactants (4% CO and 2% O_2) at the same total flow rate of 100 ml/min. The inert carrier was always Ar. The flows were controlled by thermal mass flow meters (Vögtlin Instruments). The temperature of the bed was varied between RT and 400 °C (600 °C in some cases). In this reactor the composition of the gas mixture (before and after reaction) was measured with an Agilent 7890A gas chromatograph, with a TCD detector (N_2O amount was determined through the NO and N_2 balance and confirmed by the FTIR spectra). The columns are a molecular sieve 13X (60/80 mesh, 1.8 m) and a Porapak Q (1.8 m). Calibration was done using standard gases containing known concentrations of the components.

The second set of activity measurements approaches actual conditions of an automotive exhaust. A quartz flow reactor, 6 mm ID, and a flow rate to mass of catalyst ratio = 970,000 mlSTD/h·g_{cat} were used. The gas mixtures (before and after reaction) were measured by a GC (Agilent 7820) with PPQ and MS5 packed columns in series, with backflush. Both TCD and FID detectors were used. The GC is online with the gas outlet and programmed to continuously sample the mixture, so that measurements can be collected at approx. 1 sample each 4 min. A direct-access, 0–200 amu mass spectrometer (Hiden QID-20) was also used, to measure NO. The analysis with the MS is almost continuous (0.5–1 measurement/s)

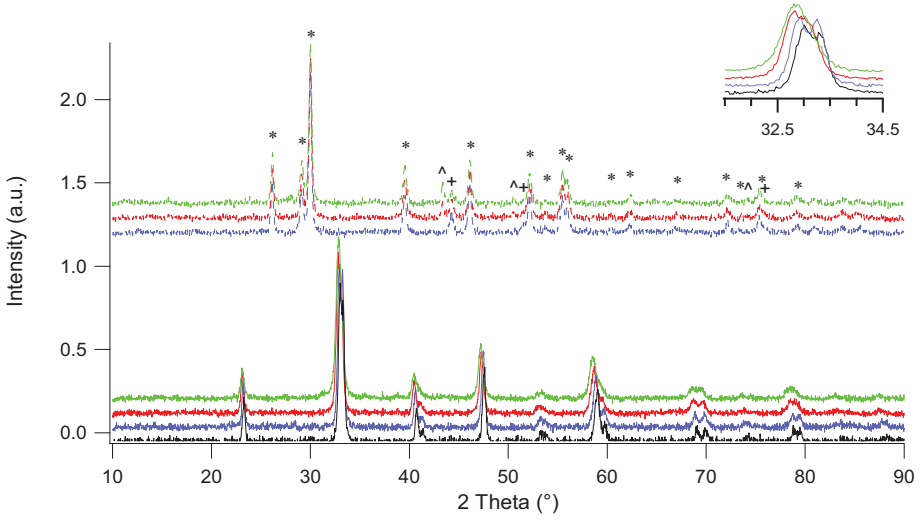

Fig. 1. XRD patterns of $LaCo_{1-x}Cu_xO_3$ samples as prepared (continuous line) and after the TPR up to 900 °C (dotted line): $x = 0$ black, $x = 0.1$ blue; $x = 0.3$ red; $x = 0.5$ green (without markers: $LaCo_{1-x}Cu_xO_3$ phase; *: La_2O_3; ⁝ Cu(0); +: Co(0)). In the insert the enlargement of the main perovskite signal is displayed. (For interpretation of the references to colour in this figure legend, the reader is referred to the web version of this article.)

The feed mixture is a complex one, that better approximates real automotive exhaust. It is summarized in Table 1. The flows were controlled by mass flow meters (Brooks and Bronkhorst). Note that stoichiometry of O_2 is based on all the fuels and the amount expected from NO conversion to N_2 and O_2. Before complete fuels combustion (typically CH_4, the more difficult to activate), also the O_2-stoichiometric mixture is in fact O_2 rich (or fuel lean). That is the motivation for limiting the investigation to stoichiometric and fuel rich conditions.

Note that 10% steam was always fed, reflecting actual conditions, quite challenging for catalysts. The standard testing sequence in the second set of measurements is: (1) heating up the catalyst at 5 °C/min to 600 °C in air, (2) two hours of pre-conditioning at 600 °C in air, (3) two hours of conditioning at 600 °C with the reacting mixture, (4) slow temperature decrease (−1 °C/min) to measure the catalyst activity at different temperatures, and produce the conversion, X(T), profiles. It has been verified that a cooling rate of 1°/min is sufficiently slow to achieve steady-state operation of the catalyst, at each temperature scanned.

3. Results and discussion

3.1. Chemical and structural characterization

All the materials prepared are listed in Table 2. The perovskite phase with rhombohedral geometry is observed in all the $LaCo_{1-x}Cu_xO_3$ samples (JCPDS number 01-084-0848), independently of the Cu content (Fig. 1). No minor phases are observed. With copper content, a notable shift of XRD signals to lower angle values is evident suggesting the increase of unit cell parameters. The shift is rather linear with increasing the copper content (see insert in Fig. 1) being slightly lower for the sample with $x = 0.5$. The increase of the unit cell parameters is further corroborated by the structure refinement obtained using the Rietveld method, as listed in Table 2. This effect is caused by copper ionic radius, slightly higher than cobalt's one (0.73 Å against 0.63 Å) [28] and demonstrate that copper is inside the perovskite crystalline cell. Cu-doping also influences the crystallite dimensions, which decrease with copper amount.

BET surface area values are between 10 and 17 m^2/g (Table 2); copper addition causes the increment of the specific surface area.

SEM image of $LaCoO_3$ shows a porous foam-like structure with spheroidal particles (Fig. 2). The porosity of the structure reduces with the increase of copper content; $LaCo_{0.5}Cu_{0.5}O_3$ shows a slightly more compact structure, with smaller particles.

The La 3d XP peaks (Fig. 3) are characteristic of La(III), (shake-up structures at 837.7–837.9 and 854.5–854.7 eV) [43–45]. Two components are observed in the La $3d_{5/2}$ signal: at 833.4–833.6 and 834.6–834.9 eV; the comparison with literature data suggests their attribution to the perovskite (833.2 eV) [46–47] and to species such as $La(OH)_3$ (835.0 eV) and LaOOH (834.8 eV) [43–45,48–50]. The only difference observed as a function of the Cu content is a slightly higher amount of the hydroxide species (contribution around 834.8–835.0 eV) in the sample with $x = 0.5$. In the Co 2p spectra (Fig. 3) both the peak positions (779.8 and 795.3 eV) and shape (absence of the shake-up contribution at about 786–788 eV) are consistent with the presence of Co(III) [39,43–45,48]. This result is particularly relevant because it suggests the absence of Co(II) in the outmost layers. In the Cu $2p_{3/2}$ spectral region (Fig. 3), the peak positions (934.0 eV) and the shake-up signal (942 eV) characteristic of Cu(II) in perovskite are evident [39,48,51] (a tail toward lower BEs agrees with the possible presence of traces of copper in lower oxidation state). In the $LaCo_{0.5}Cu_{0.5}O_3$ catalyst the Cu $2p_{3/2}$ signal is shifted at lower BE (from 934.7 to 933.5 eV); this shift suggests the formation of low amount of highly dispersed CuO (CuO is never

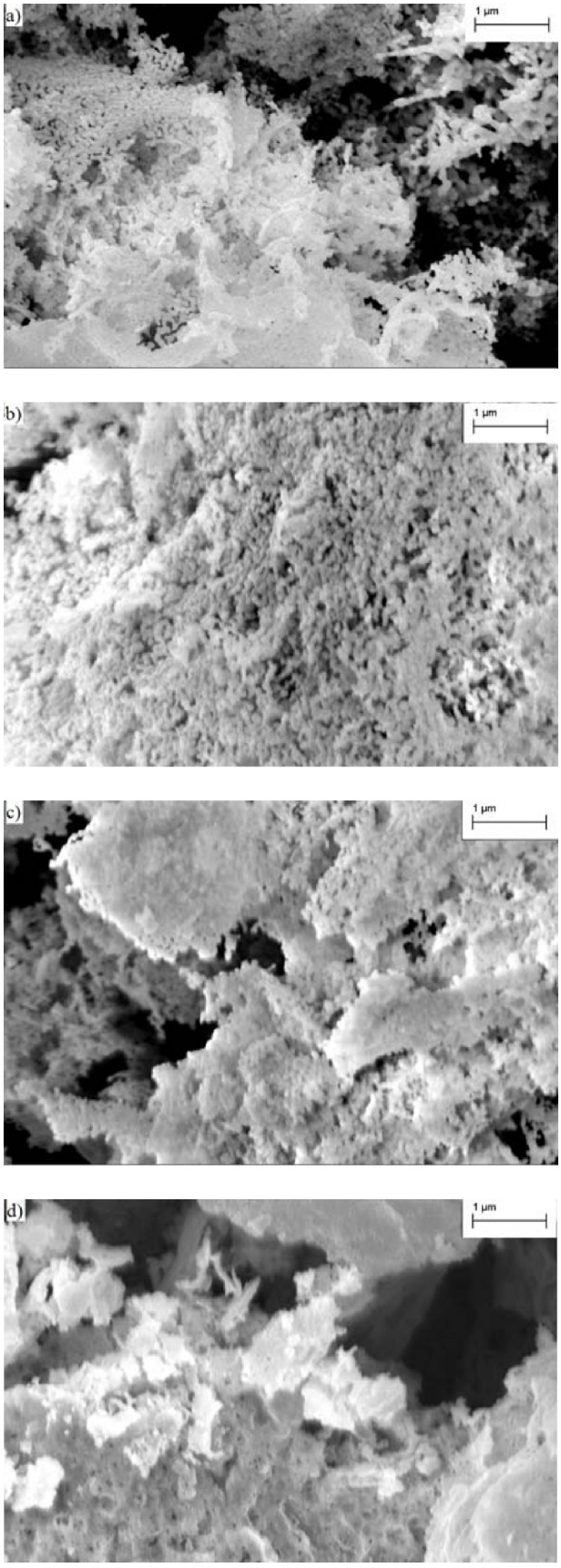

Fig. 2. SEM images of the $LaCo_{1-x}Cu_xO_3$ catalysts: a) $x = 0$, b) $x = 0.1$ c) $x = 0.3$; d) $x = 0.5$.

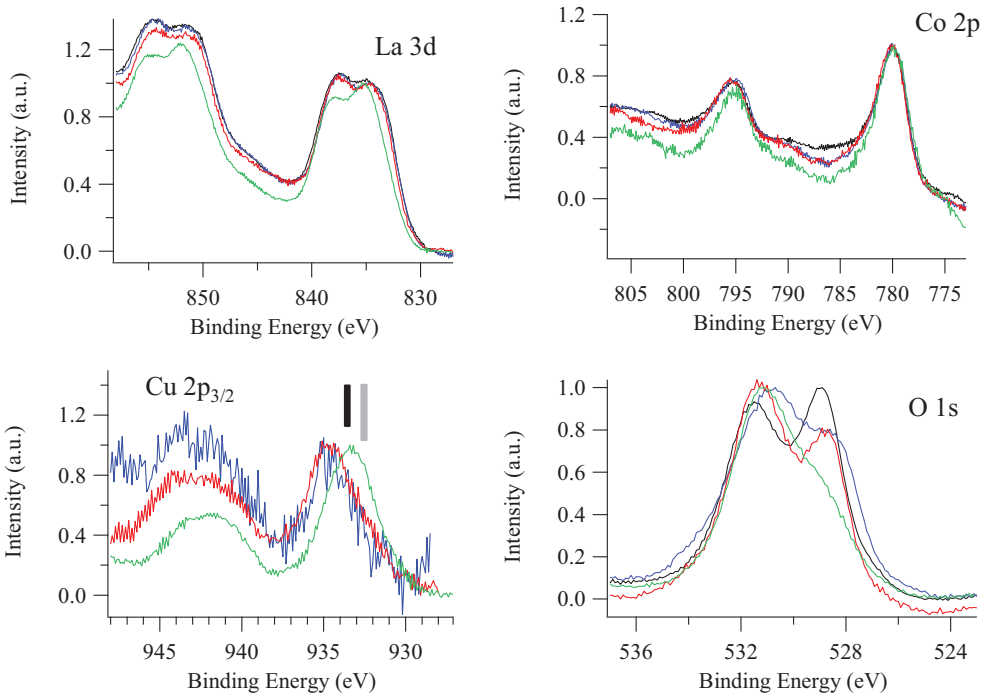

Fig. 3. La 3d, Co 2p, Cu 2p and O 1 s XPS spectra obtained for $LaCo_{1-x}Cu_xO_3$ with $x = 0$ (black), 0.1 (red), 0.3 (blue), and 0.5 (green); the spectra are normalised for an easier comparison. The range of Binding Energies reported in literature [48] for Cu(II) in CuO (black) and for Cu_2O and Cu(0) (grey) are also indicated. (For interpretation of the references to colour in this figure legend, the reader is referred to the web version of this article.)

observed in the XRD patterns) consistently with the lower shift in the XRD signal. The presence of traces of copper in lower oxidation states can not be excluded (Cu_2O, as an example, however the only way to distinguish between Cu(I) and Cu(0) is from the Auger signal whose s/n ratio is rather low). Two main signals compose the O 1 s spectra (Fig. 3): the peak at 528.8–529.1 eV is due to the perovskitic oxygen whereas the one at 531.3–532.0 eV at oxygen in hydroxides and carbonates [39,43–45,48]. The signal due to perovskitic oxygen is lower than that of hydroxides in the sample with $x = 0.5$ confirming a more abundant amount of hydroxide/carbonate species.

XPS quantitative analysis (Table 3) reveals that oxygen is always overstoichiometric due to the surface hydroxylation and carbonation. A surface segregation of lanthanum is evident (Table 4). This phenomenon, which is maximum in the undoped $LaCoO_3$, is also particularly evident in the sample richer in Cu: $LaCo_{0.5}Cu_{0.5}O_3$ (Table 4, La/(Cu + Co) atomic ratio is about 2.8). The Cu/Co XPS atomic ratio is always higher than the nominal one, suggesting a surface segregation of copper with respect to cobalt.

3.2. Temperature programmed reduction

The TPR of $LaCoO_3$ (Fig. 4) reveals two signals at 440 and 598 °C. Accordingly with literature data [3,52–57] the signal at 440 °C is attributed to the reduction from Co(III) to Co(II) and the peak at 598 °C to the reduction of Co(II) to Co(0).

In the TPR profiles of the $LaCo_{1-x}Cu_xO_3$ two main peaks are observed at 380–440 °C and 460–600 °C and a shoulder around 300–320 °C becomes evident for $x = 0.3$ and $x = 0.5$. Literature data [28,58] indicate a two-step reduction also for Cu-doped cobaltates as for undoped lanthanum cobaltate: from Co(III) to Co(II) and from Cu(II) to Cu(0) at 310–380 °C and from Co(II) to Co(0) at 380–540 °C. However, an interesting behaviour is sometime observed for copper cations, as a function of composition [59]: a two-steps reduction with Cu(I) as intermediate when copper is present in low amounts and a single step reduction, similarly to what observed for copper

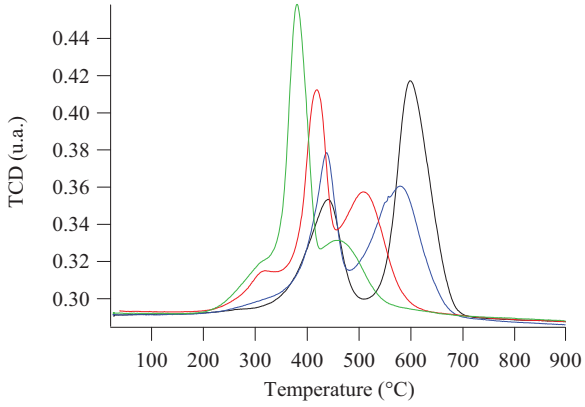

Fig. 4. TPR profiles of $LaCo_{1-x}Cu_xO_3$ with $x = 0$ (black), $x = 0.1$ (blue), $x = 0.3$ (red) and $x = 0.5$ (green). (For interpretation of the references to colour in this figure legend, the reader is referred to the web version of this article.)

oxide but at a lower temperature (270 instead of 330 °C), in Cu-rich perovskites.

Focusing on our results, the reduction temperature was observed to decreases with increasing copper content; moreover, increasing the Cu amount, from $x = 0.1$ to $x = 0.5$, the intensity of the signal at higher temperature decreases and the intensity of the peak at lower temperature increases. These results suggest to attribute the shoulder at 300–320 °C to the Cu(II) → Cu(I) reduction and the signal at 380–440 °C to the reduction of Cu(I) to Cu(0) and to the first step of cobalt reduction. The peak at 460–600 °C is due to the reduction of Co(II) to Co(0).

Consistently with this attribution, no significant differences are observed between the XRD patterns of the as-prepared sample and of those of the sample after the TPR carried out up to about 330 °C [36] whereas cubic Cu(0) is observed in the pattern of the samples treated at 420–480 °C (i.e. after the reduction at 380–440 °C). In addition to the copper cations reduction, a slight shift of the peaks

Table 3
XPS atomic compositions obtained for $LaCo_{1-x}Cu_xO_3$ ($0 \le x \le 5$) perovskites. The nominal compositions are reported for comparison.

	$x=0$		$x=0.1$		$x=0.3$		$x=0.5$	
	XPS	Nominal	XPS	Nominal	XPS	Nominal	XPS	Nominal
La	19	20	19	20	20	20	21	20
Co	5	20	9	18	7	14	3	10
Cu			1	2	5	6	4	10
O	76	60	72	60	69	60	71	60

toward lower angles, consistent with a cell parameters increment and thus with the reduction from Co(III) to Co(II), can be observed; in contrast no signals corresponding to other phases are observed. This reduction is thus obtained without the collapse of the main perovskite structure: the only consequence being the increment of the crystallographic cell due to the partial conversion of Co(III) into Co(II). Tien-Thao et al. [28,29] observed, upon reduction at 375 °C, the formation of the orthorhombic $La_2(Co_{0.75}Cu_{0.25})O_{4.2}$ perovskite, in addition to $LaCoO_3$, and metallic copper. This phase was not observed in our samples. The XRD pattern recorded after the TPR until 900 °C (Fig. 1) reveals the formation of cubic Cu(0), cubic Co(0), hexagonal La_2O_3, and traces of orthorhombic La_2CoO_4.

As mentioned above, reduction temperatures shift at lower values with increasing copper content: from 598 °C ($x=0$) to 459 °C ($x=0.5$), and from 440 °C ($x=0$) to 380 °C ($x=0.5$). The decrease of the reduction temperature with increasing copper content was already observed in literature. Tien-Thao et al. [28,29] hypothesized that under reducing conditions copper diffuses toward the surface acting as a catalyst for hydrogen dissociation. This causes the decrease of the Co(III) reduction temperature, particularly for the grain boundaries cobalt species.

For all the catalysts except $LaCo_{0.5}Cu_{0.5}O_3$ the measured hydrogen consumptions are slightly lower than the expected values (Table 5). The XRD patterns recorded after the TPR (Fig. 1) allow excluding the presence of residual un-reduced species. The slightly lower consumption suggests thus the presence of traces of Co(II) in the powder bulk (no traces of Co(II) are revealed by XPS) and/or of Cu(I). However it is interesting to observe that in the sample richer in copper the measured and calculated H_2 consumptions are equals, allowing to exclude a significant presence of Cu(I) and Co(II). Taking into consideration the catalysts with $x=0.1$ and $x=0.3$, the relative amounts of consumed H_2 confirm the following attribution: 300–320 °C Cu(II) → Cu(I); 380–440 °C Cu(I) → Cu(0) and Co(III) → Co(II); 460–600 °C Co(II) → Co(0). In contrast, the relative intensity of the signals at higher temperature in the Cu-richer catalysts suggests that: (i) partial reduction of Co(II) also takes place at 380–440 °C; (ii) a significant part of copper (60% of the total) is reduced to Cu(0) in a single step contributing to the signal at 380–440 °C.

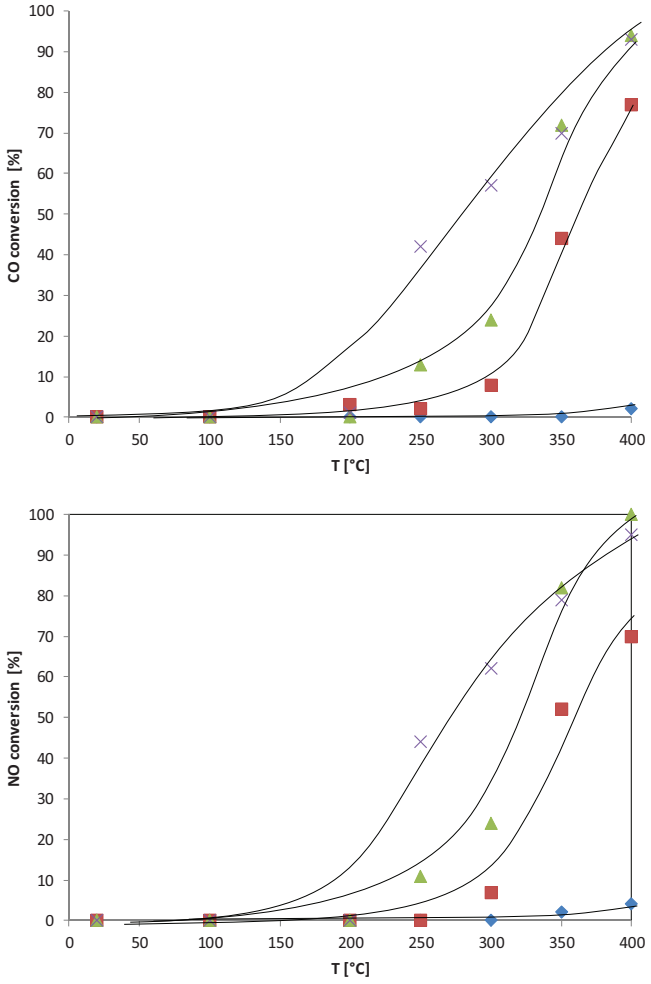

Fig. 5. CO (above) and NO (below) conversion as a function of temperature ×:$LaCo_{0.5}Cu_{0.5}O_3$ ▲:$LaCo_{0.7}Cu_{0.3}O_3$ ■:$LaCo_{0.9}Cu_{0.1}O_3$ ♦:$LaCoO_3$.

3.3. Reactivity

3.3.1. Reactivity with CO + NO

The catalytic tests with CO + NO mixtures were performed using stoichiometric amounts of CO and NO. Fig. 5 shows the CO and NO conversion as a function of temperature for all the catalysts. At these conditions, all the copper-doped samples reach a almost complete conversion at 400 °C of both CO and NO whereas the activity of $LaCoO_3$ is quite poor, barely perceivable even at 400 °C. Results indicate that the conversion at a given temperature increases in the order $LaCoO_3 < LaCo_{0.9}Cu_{0.1}O_3 < LaCo_{0.7}Cu_{0.3}O_3 < LaCo_{0.5}Cu_{0.5}O_3$ i.e. with larger Cu doping. Note that the activity of $LaCo_{0.5}Cu_{0.5}O_3$ is significantly higher than the other Cu-doped $LaCoO_3$, at lower temperatures, with conversion in excess of 40% for both CO and NO already at 250 °C. The reactivity of the other copper containing

Table 4
XPS atomic ratios obtained for $LaCo_{1-x}Cu_xO_3$ ($0 \le x \le 5$) perovskites. The nominal ratios are reported for comparison.

	$x=0$		$x=0.1$		$x=0.3$		$x=0.5$	
	XPS	Nominal	XPS	Nominal	XPS	Nominal	XPS	Nominal
Cu/Co	0.0	0.0	0.2	0.1	0.7	0.4	1.4	1.0
La/(Cu + Co)	4.1	1.0	1.9	1.0	1.7	1.0	2.8	1.0

Table 5
Estimated and measured hydrogen consumption values as a function of the copper content; the relative amount of the reduction signals (determined by fitting procedure) is also reported.

Sample	Estimated consumpion(cm^3/g)	Measured consumption(cm^3/g)	300–320 °C	380–440 °C	460–600 °C
$LaCoO_3$	136.69	130.82	–	33	67
$LaCo_{0.9}Cu_{0.1}O_{2.95}$	132.32	126.22	5	33	62
$LaCo_{0.7}Cu_{0.3}O_{2.85}$	123.53	119.99	9	47	44
$LaCo_{0.5}Cu_{0.5}O_{2.75}$	114.70	114.94	8	63	29

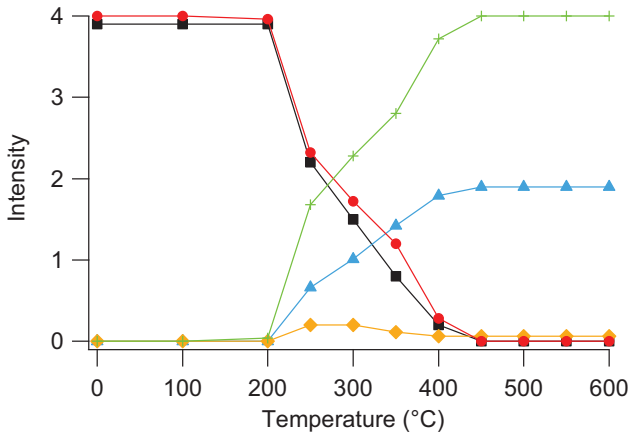

Fig. 6. Concentrations of CO (red balls), NO (black squares), CO_2 (green crosses), N_2 (light blue triangles), and N_2O (orange rhombs) measured, for $LaCo_{0.5}Cu_{0.5}O_3$ at different temperatures in the reaction NO + CO. (For interpretation of the references to colour in this figure legend, the reader is referred to the web version of this article.)

samples ($x = 0.3$ and $x = 0.1$) requires at least 300–350 °C to become significant.

Note that CO and NO conversion are quite similar, as expected from a direct reduction of an equimolar mixture.

The reaction with the most active catalyst ($LaCo_{0.5}Cu_{0.5}O_3$) was also monitored with FT-IR spectroscopy on the products, for a better understanding of the reaction mechanism. FT-IR can simultaneously detect NO, N_2O and NO_2, indicating whether NO oxidation or reduction prevail. Four main contributions are evident (Fig. S1): the stretching of N—O bond in NO (centered at 1875 cm^{-1}), the contribution of N_2O asymmetric stretching (centered at 2225 cm^{-1}), the stretching of C—O bond in CO (centered at 2143 cm^{-1}) and the contribution of CO_2 asymmetric stretching (centered at 2350 cm^{-1}). Focusing on N_2O contribution at 2225 cm^{-1}, it can be seen that its formation begins at about 200–250 °C; its signal intensity decreases at higher temperature, suggesting the decomposition of N_2O to N_2 and O_2. The amounts of the different reaction products, compared in Fig. 6, confirms that N_2 is the main reaction product of NO decomposition while N_2O is an intermediate product that decreases at increasing temperature. The formation of NO_2 species, revealed by intense bands around 1600 cm^{-1} is never observed; only at RT two signals at 1631 and 1598 cm^{-1}, attributed to these species, are evident. The obtained results are consistent with the mechanism proposed in literature for CO + NO reaction over several perovskite surfaces, among which $LaCo_{1-x}Cu_xO_3$ obtained by reactive grinding [31,32], and allows to exclude complex mechanisms considering the formation of intermediate N_xO_y species operating as oxidizing agent (as an example for hydrocarbons) [18], [60–62]. This mechanism takes into consideration several steps:

adsorptions

$$NO_g \rightarrow NO_{ads} \quad (1)$$

$$CO_g \rightarrow CO_{ads} \quad (2)$$

surface reactions

$$NO_{ads} \rightarrow N_{ads} + O_{ads} \quad (3)$$

$$N_{ads} + NO_{ads} \rightarrow N_2O_{ads} \quad (4)$$

$$CO_{ads} + O_{ads} \rightarrow CO_{2,g} \quad (5)$$

$$N_2O_{ads} \rightarrow N_{2,g} + O_{ads} \quad (6)$$

$$N_2O_{ads} + CO_{ads} \rightarrow N_{2,g} + CO_{2,g} \quad (7)$$

desorptions

$$2N_{ads} \rightarrow N_{2,g} \quad (8)$$

$$N_2O_{ads} \rightarrow N_2O_g \quad (9)$$

$$2O_{ads} \rightarrow O_{2,g} \quad (10)$$

Some considerations on this mechanism allow to better understand the role played by copper doping in the reactivity of the $LaCoO_3$.

Taking into consideration the adsorption steps (1 and 2), Tascón et al. [63] observed on $LaCoO_3$ and $LaMnO_3$, that NO chemisorption inhibits subsequent CO chemisorption more than the reverse (CO chemisorption inhibiting NO chemisorption) thus suggesting that CO affinity for these surfaces is weaker than NO. Zhang et al. [31] made similar considerations for $LaCo_{0.8}Cu_{0.2}O_3$. Moreover, Chupin et al. [64] observed that in cobalt containing catalysts, NO interacts with Co(II) surface sites which are not abundant in cobalt containing oxides (Co(III) is prevailing, as also confirmed by XPS results). Taking into consideration these aspects the reactivity of $LaCoO_3$ with respect to NO reduction is expected to be low so justifying the Cu-doping. At first it has to be considered that copper doping increases the specific surface area and this can positively affect the reactivity. However, the comparison between specific surface area and conversion values suggests that this increment is not the main responsible of the reactivity increment (the increment in reactivity is not linear with the increment in specific surface area; moreover, the conversion values measured for $LaCo_{0.9}Cu_{0.1}O_3$ and $LaCo_{0.7}Cu_{0.3}O_3$ are different whereas specific surface area is the same).

At low temperatures the Rate Determining Step (RDS) of the catalytic reduction of NO by CO on perovskites, and particularly on copper doped lanthanum cobaltites, is considered to be the dissociative adsorption of NO with the formation of N_2 and/or N_2O (steps 3 and 4), [31]. Hence, the global activity can be connected with the availability of adsorption sites for dissociative chemisorption of NO on the surface of the catalyst. In particular, unlike metallic catalysts, the first step in the perovskite catalysed NO reduction, is the interaction of NO with a lattice oxygen vacancy which provides enough energy for the N—O bond breakage [65].

The presence of copper inside the perovskite structure is determinant for the formation of oxygen vacancies, providing adsorption sites for NO and promoting the rate determining dissociation of NO adsorbed species. Zhou et al. [66] carried out DFT calculations on Cu-doped $LaCoO_3$, using plane waves as implemented in Vienna ab-initio simulation package. They demonstrated that Cu doping decreases the energy of oxygen vacancy formation near Cu sites, suggesting their spontaneous formation. Moreover, copper cations

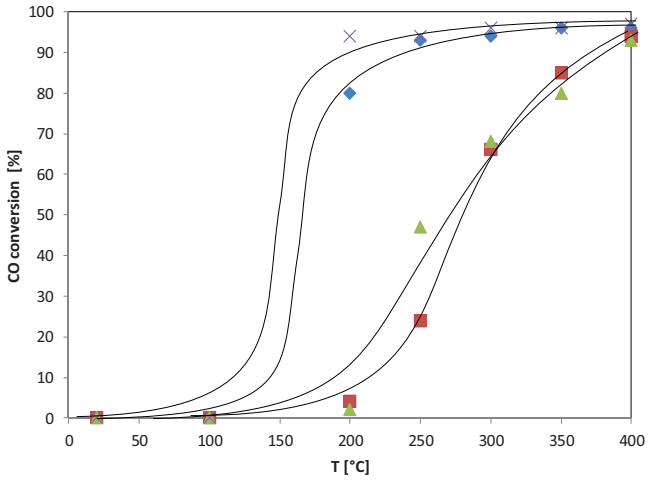

Fig. 7. CO conversion as a function of temperature in $CO+O_2$ reaction. ×:$LaCo_{0.5}Cu_{0.5}O_3$ ▲:$LaCo_{0.7}Cu_{0.3}O_3$ ■:$LaCo_{0.9}Cu_{0.1}O_3$ ♦:$LaCoO_3$.

are expected to coordinate two NO molecules forming a dinitrosyl specie that decomposes forming N_2 and/or N_2O [31,65]. The NO dissociation can also involve the formation of the dimeric species (N_2O_2) as intermediate; in this case the formation of N_2O is much easier only involving a N—O bond breaking whereas the formation of N_2 should result from two bonds cleavages. It is interesting to observe, as summarized by Centi et al. [65], that the presence of Cu(II) and/or Cu(I) appears to deeply affect the formation of dynitrosyl species. Consistently, the TPR results suggest for copper an active role in the reduction reaction.

Once formed the N_2O can decompose to N_2 and O_2 (step 6) or react with the CO, giving rise to N_2 and CO_2 (step 7), the first path being rather difficult on $LaCo_{1-x}Cu_xO_3$ perovskites at temperature lower than 300 °C. [31]

3.3.2. *Reactivity with CO + O_2*

The catalytic activity in CO oxidation was evaluated using a stoichiometric mixture of CO and O_2 (4 and 2%, respectively). Fig. 7 compares the CO conversion as a function of temperature achieved by all the $LaCo_{1-x}Cu_xO_3$ prepared. $LaCoO_3$ activity as an oxidation catalyst was already known. The surprising result is the comparable (slightly higher than $LaCoO_3$) activity of $LaCo_{0.5}Cu_{0.5}O_3$, resulting the most active catalyst in the series, reaching 97% of conversion at 400 °C. Its activity is already extremely high at 200 °C, peaking at 94% CO conversion. Such an activity remains also at higher temperature. Differently, $LaCo_{1-x}Cu_xO_3$ with $x = 0.1$ and $x = 0.3$ are inactive below 200 °C; their activity becomes significant only above 250 °C and at 400 °C exceeds 90%.

It is usually accepted that the CO oxidation proceed via Mars-van Krevelen mechanism. CO molecularly adsorbs on Lewis surface acidic sites (step 2) and reacts with oxygen species near neighbors of the Lewis acidic sites originating CO_2 that desorbs (step 5). The result is a partially reduced site (oxygen vacancy) that may be re-oxidized by gas phase oxygen or deactivate by interacting with CO; the interaction with another adsorbed CO can also give rise to CO_2 and C. This mechanism was confirmed among others by Xu et al. [67] who investigated the catalytic oxidation of CO by N_2O and O_2 on a Co_3O_4 (1 1 0) surface. The DFT calculation demonstrated that, in this case, N_2O can interact with the oxygen vacancy site to regenerate the surface, releasing N_2.

In Co_3O_4 CO was suggested to bind with the carbon end to Co(III) ions in the top layer [68,69]. The behavior of cobalt oxide species seems, moreover, to be affected by the cluster size as indicated by Xie et al. [70] who investigated the reaction of oxide clusters with CO, NO, C_2H_2, and C_2H_4 by means of time of flight mass spectrometry and DFT calculations. Yan Xie et al. suggested that the reactivity in oxidation is strongly related to the cluster size, the number of cobalt atoms in high oxidation state, the O—O bonding in the oxide clusters and underlined the possible interaction with Co(II) species. This result is particularly important because Co(III) cationic species are certainly prevailing in real catalyst surfaces, as confirmed by XPS, even if the formation of Co(II) sites can not be excluded in reducing conditions. In the present case the more active catalysts are $LaCoO_3$ and $LaCo_{0.5}Cu_{0.5}O_3$, which are characterized by a marked surface segregation of Lanthanum as observed by XPS (La/(Cu + Co) atomic ratio = 4.1 and 2.8, respectively); CO can thus be suggested to interact with La surface Lewis acidic sites. The interaction of CO with La(III) surface Lewis acidic sites was already observed by Natile et al. [71] comparing the interaction of CO with $LaCoO_3$ powders obtained by means of different preparation procedures, with a Co_3O_4/La_2O_3 composite, and with La_2O_3. The obtained results indicate a strong interaction between CO and La_2O_3. A severe hydroxylation was observed (XPS) in the sample with $x = 0.5$; around 200 °C a significant desorption of water is observed in copper doped $LaCoO_3$ [36] and the formation of new La(III) Lewis acidic sites on surface is expected. CO chemisorbs molecularly on these new acidic sites. Once CO is chemisorbed on the catalyst surface, it is converted to CO_2 by means of the lattice oxygen (Mars-van Krevelen mechanism). To this purpose, Cu doping can be of great help inducing the formation of oxygen vacancies and thus increasing the oxygen ions mobility [28]. Focusing on the CO_2 desorption, the possibility of the surface cations reduction is crucial [69]. As revealed by TPR results the doping with Cu increases the catalyst reducibility (Co(III) to Co(II), as an example, but also Cu(II) to Cu(I) or Cu(0)) and is expected to favor also the step 5. Surface poisoning by interaction with CO_2 is observed, as an example, in $CoAl_2O_3$ in which Co and Al assume oxidation states II and III, respectively: neither one of these ions is likely to be reduced upon surface oxygen abstraction and step 5 is not allowed anymore. Summarizing, the reactivity in CO oxidation requires the interaction between CO and surface active Lewis acidic sites (La(III) cations, for example), the conversion of CO into CO_2 by means of the perovskite lattice oxygen, the desorption of the adsorbed CO_2 with surface cations reduction, and the perovskite surface re-oxidation (with the reactive mixture oxygen). Cu doping affects the surface composition: the segregation of lanthanum and thus the presence of La(III) surface active Lewis acidic sites is observed to decrease with the following order: $LaCoO_3 > LaCo_{0.5}Cu_{0.5}O_3 > LaCo_{0.9}Cu_{0.1}O_3 = LaCo_{0.7}Cu_{0.3}O_3$) and consistently is expected to decrease the interaction between CO and surface. Copper doping causes the decrease of the surface Lewis acidic sites and thus un-favors the interaction of CO with the catalyst surface. This effect is not linear with the nominal composition being less evident in the sample richer in copper. The addition of copper, however, increases the oxygen mobility [28] and the catalyst reducibility. Oxygen mobility is important since a higher oxygen mobility can favor the conversion of CO into CO_2. The cations reducibility is also crucial for the catalytic performance because it can facilitate the CO_2 desorption, preventing the catalyst deactivation. Both these features seem to support the reactivity and apparently compensate the lower amount of active sites for CO adsorption caused by the introduction of copper. As a matter of fact the reactivity with respect to CO oxidation is not significantly different in the undoped and highly doped catalysts.

3.3.3. *Reactivity with the complex TWC mixture*

The most active catalysts, $LaCo_{0.5}Cu_{0.5}O_3$ and $LaCoO_3$, were then tested towards the complex mixture. Considering that the behavior of this complex mixture is less obvious, it has been investigated up to higher temperature, i.e. 550 °C. The presence of higher and unsaturated hydrocarbons suggests to verify the possibility of homogeneous reactions. A blank test (empty quartz reactor, with

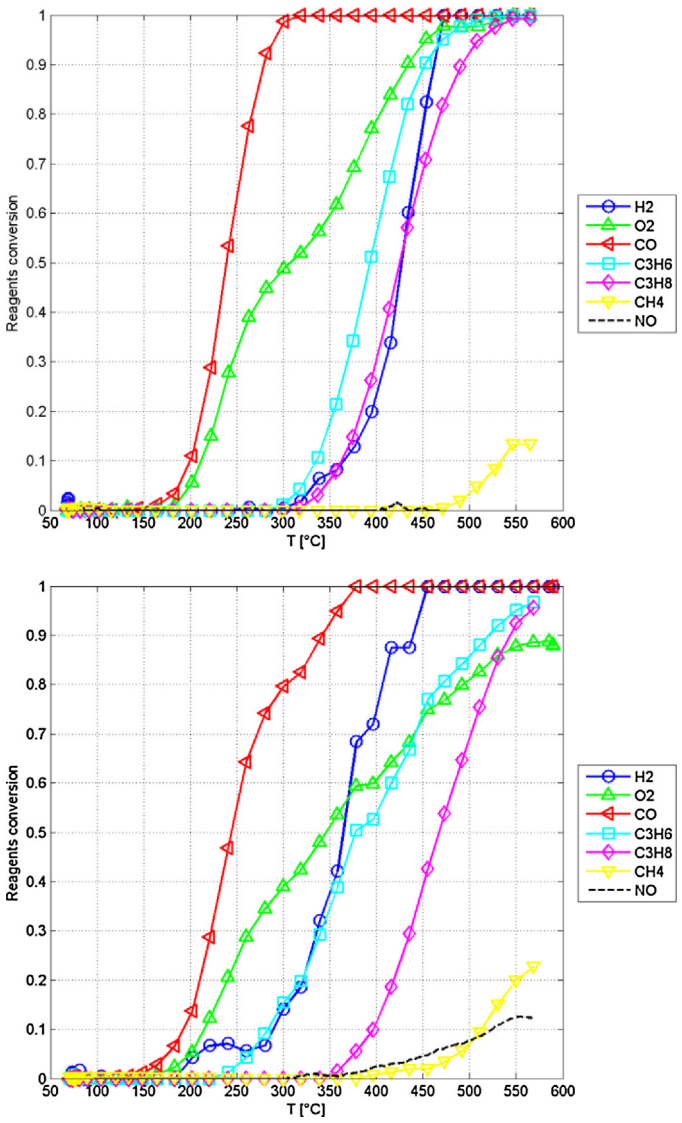

Fig. 8. Reactants fractional conversion on $LaCoO_3$ (a = above) and $LaCo_{0.5}Cu_{0.5}O_3$ (b = below) with the complex stoichiometric TWC mixture; O_2 ○:H_2 ◄:CO ▲:O_2 □:C_3H_6 ◊:C_3H_8 ▼:CH_4 –:NO.

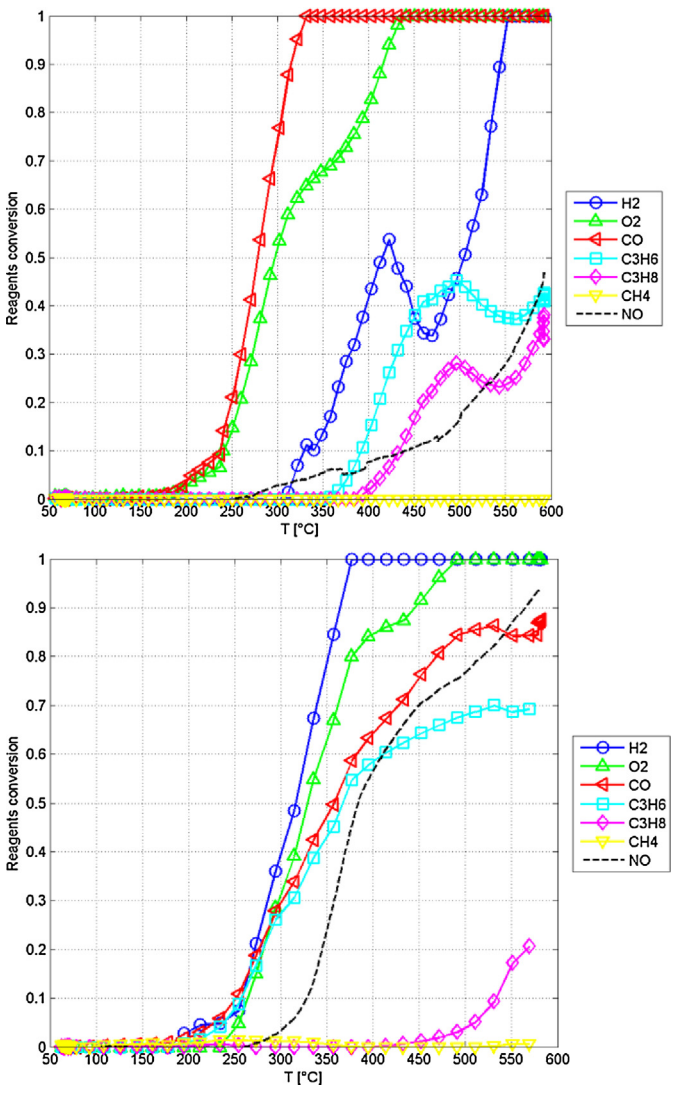

Fig. 9. Reactants fractional conversion on $LaCoO_3$ (above) and $LaCo_{0.5}Cu_{0.5}O_3$ (below) with a complex fuels-rich mixture (O_2 deficient). ○:H_2 ◄:CO ▲:O_2 □:C_3H_6 ◊:C_3H_8 ▼:CH_4 –:NO.

quartz wool plugs later used to hold the catalysts), confirms the absence of any homogeneous reaction up to 550 °C. While not obvious, it could be explained by the quenching of any initiating radical by the large amount of H_2O and CO_2, and the abundance of surface per unit volume provided by the quartz wool. This is favorable to better highlight the catalytic properties of the perovskites. A similar test (not show) on a bare cordierite monolith, without any catalyst on it, showed that the supposedly 'inert' support causes approx. 30% C_3H_6 and C_3H_8 conversion at 600 °C.

Two different mixtures (Table 1) have been tested. In the stoichiometric one, the O_2 fed and the O_2 expected from NO conversion to N_2 and O_2, exactly balance the O_2 required by fuels (CO, H_2, HCs) to achieve total oxidation. In practice, not all the species react simultaneously, at a given temperature, so that O_2 rich/lean condition may prevail at different temperatures, even if a stoichiometric O_2 is used.

The results for the 'stoichiometric' mixture are shown in Fig. 8 for the most promising $LaCo_{0.5}Cu_{0.5}O_3$ and compared with the well-established $LaCoO_3$. The latter, Fig. 8a, shows excellent oxidation properties for CO, as frequently reported in the Literature, since [1], where the $LaCoO_3$ activity for oxidation is usually tested with just CO. $LaCoO_3$ is not equally active in oxidizing C3's, requiring approx. an extra 150 °C, and almost ineffective for CH_4 oxidation, achieving only 15% conversion at 550 °C. Interestingly, $LaCoO_3$ does not differentiate the reactivity of saturated and unsaturated C3s, and also H_2 is not easily burnt, as would be expected. Note that the O_2 conversion is predominantly determined by the CO consumption, which is the most abundant reactant; at total CO conversion, the O_2 conversion is almost 50%, consistently with the initial stoichiometry. Finally, NO reduction is very scarce on $LaCoO_3$ when O_2 rich conditions prevail, even if is not in large excess. Comparative results for $LaCo_{0.5}Cu_{0.5}O_3$ are reported in the same Fig. 8b. The addition of Cu has kept the oxidation activity for CO, made H_2 oxidation easier, differentiated the C3s oxidation, where the unsaturated C_3H_6 reacts more easily (lower temperature) than its corresponding alkane. This can be consistent with the ease of H_2 activation, consistent with the presence of surface Cu(0). Unfortunately, NO reactivity remains very low. As said, we believe that the reducing properties of Cu are contrasted by an excess O_2 in the partially reacted mixture.

A totally different behavior is observed with a fuel-rich mixture, Fig. 9. The good activity of $LaCoO_3$ in oxidizing CO is still present (Fig. 9a), although approx. an additional 50 °C are required

Table 6
XPS atomic compositions obtained for $LaCo_{0.5}Cu_{0.5}O_3$ perovskites before and after reactivity. The nominal compositions are reported for comparison.

	Before reaction		After reaction CO + ½ O_2	After reaction CO + NO	After reaction TWC mixture
	XPS	Nominal	XPS	XPS	XPS
La	21	20	17	19	13
Co	3	10	3	4	4
Cu	4	10	9	4	12
O	71	60	71	73	71

to achieve the same conversion measured with excess O_2; it suggests that a major role in CO activation on $LaCoO_3$ is played by lattice oxygen, quite independently from the O_2 available in the reacting mixture, consistently with the already mentioned Mars-van Krevelen mechanism. Some better NO conversion is noticed, up to 50% at 600 °C, but still unsatisfactory for TWC purposes, both for the conversion degree and the high temperature required. The lack of O_2 generates a competition between H_2 and C3s for its use. The activity order that emerges is $H_2 > C_3H_6 > C_3H_8$, as expected. Still, the maximum activity in C3s oxidation appears to compete with H_2, causing some regression in its conversion, in the 430–500 °C range.

Comparative results for $LaCo_{0.5}Cu_{0.5}O_3$ are reported in the same Fig. 9b. H_2 is now the species that oxidize at the lowest temperature, seizing O_2 so that complete CO conversion cannot be achieved (it is limited by the total consumption of O_2 above 480 °C). Early consumption of the limiting O_2 is also supported by the low temperature reactivity of C_3H_6. Again, the reactivity order $H_2 > C_3H_6 > C_3H_8$ is clear, but it is quite extreme when O_2 is scarce, deferring the C_3H_8 conversion to very high temperature; even above 550 °C C_3H_8 is approx. 20% and likely due to cracking, since O_2 is totally missing. CH_4 is not reacting at all, up to 600 °C. However, we finally measured on $LaCo_{0.5}Cu_{0.5}O_3$ a very good NO conversion, starting at fairly low temperature and approaching 100%. Note that NO conversion boosts after the total consumption of O_2, confirming that O_2 is a major obstacle to NO decomposition catalysts, even if a reducing functionality is incorporated in their structure. This result is consistent with the mechanism observed with CO + NO mixture, that considers the dissociative interaction of NO with oxygen vacancy sites the RDS for NO reduction. However, the self deactivation of copper species for nitrate formation observed by Centi et al. [72] should be considered as another possible cause as well as the consumption of reducing species (such as CO) that are oxidized by oxygen.

Note that the testing of catalyst activity with the complex mixture, leading to the results of Figs. 8 and 9, is carried while cooling, after a catalyst conditioning in air at 600 °C, as described above (Section 2.3). Accordingly, the catalyst reduced forms highlighted by TPRs are never expected, because H_2 and CO are likely to be in contact with the catalyst without reacting with O_2 in the gas mixture only at a temperature below the lower TPR peak.

3.3.4. *Reacted catalysts characterization*

The XPS analysis carried out on the $LaCo_{0.5}Cu_{0.5}O_3$ catalyst after CO + NO, CO + 1/2 O_2, and TWC reactions are reported in Fig. 10 and Table 6. After CO + NO and TWC the formation of nitrogen containing species on the surface is not observed; a similar result

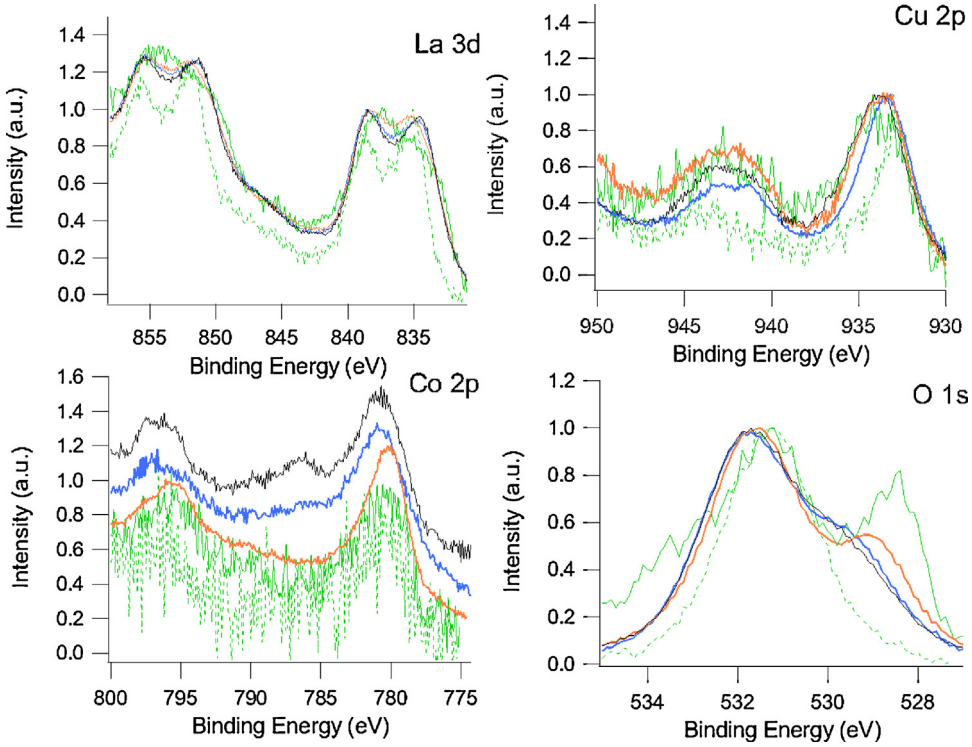

Fig. 10. La 3d, Co 2p, Cu 2p and O 1 s XPS spectra obtained for $LaCo_{0.5}Cu_{0.5}O_3$ before reaction (green continuous line) and after the following reactions: CO + 1/2 O_2 (orange), CO + NO (blue), TWC mixture (black). The spectra obtained after the TPR experiment (green dotted line) are also reported for comparison. The spectra are normalized with respect to their maximum value for comparison. (For interpretation of the references to colour in this figure legend, the reader is referred to the web version of this article.)

was obtained when the CO + NO reaction was carried out inside a DRIFT reaction chamber. These results exclude the possibility of the surface deactivation by nitrate formation. The XPS composition determined on the reacted samples, Table 6, reveals that both the reaction with CO + ½ O_2 and with the TWC mixture cause the decrease of lanthanum and the increment of copper, whereas the CO + NO mixture does not cause significant variation of the catalyst surface. The comparison among the XPS O 1 s signals, Fig. 10, reveals that the reaction causes the decrement of the contribution due to the perovskitic oxygen (around 528.5 eV) whereas a new shoulder around 529–530 eV, attributed to oxygen bound to cobalt and copper is evident; this shoulder is less intense with respect to the contribution due to the formation of hydroxide and carbonate groups (531.5–532.0 eV). No significant differences have been observed in the peaks of the other elements, Fig. 10, the more relevant being the slight reduction of cobalt after the exposure to the TWC mixture. This reduction is revealed by the small shake-up contribution due to Co(II) observed at about 786 eV.

4. Conclusions

In this work copper doped lanthanides have been investigated with the aim of extending their applicability as automotive catalysts: to this aim both the reactivity in model reactions (CO + NO and CO + 1/2O_2) and with complex mixtures simulating automotive exhaust under lean and rich conditions, has been investigated. Four powders with nominal composition $LaCo_{1-x}Cu_xO_3$, (x = 0, 0.1, 0.3, 0.5) have been synthesized by means of the citrate method. XRD patterns indicate that a stable perovskitic phase with rhombohedral geometry has been obtained for all the compositions. The crystallite size decreases with increasing the copper amount and also the morphology differs. Temperature Programmed Reduction (TPR) measures indicate that copper causes the decrease of the Co(III) to Co(II) and Co(II) to Co(0) reduction temperature, as a consequence of the activation of H_2 due to the surface segregated copper clusters and of the increased oxygen mobility due to the formation of vacancies. X-ray Photoelectron Spectroscopy (XPS) results are consistent with the surface segregation of lanthanum as oxide/hydroxide; this phenomenon is more evident in the $LaCo_{0.5}Cu_{0.5}O_3$ thus suggesting an higher surface reactivity with respect to atmospheric moisture and carbon dioxide in this catalyst. When copper is present in high amount, x = 0.5, it segregates on the surface favoring the catalytic activity. Reactivity has been measured in simple NO + CO and CO + O_2 reactions; beside this the reactivity with respect to complex mixtures approaching automotive exhaust composition, at both stoichiometric and O_2 limiting conditions, has been studied. The results of the reactivity tests have been discussed on the basis of the Cu-doping in order to deep into the mechanism. To this end, the reacted catalysts have also been characterized. The cations play a different role in the CO oxidation and NO reduction; CO and NO coordinate to different surface active sites and their adsorption is thus depending on Cu content.

Focusing on the automotive exhaust mixture, $LaCo_{0.5}Cu_{0.5}O_3$ is interesting both in terms of oxidation and NO reduction capability but activity is severely depressed by the presence of oxygen, differently from some PGM-based commercial catalysts. The behavior observed with the automotive mixture, is investigated and discussed taking into consideration the reaction mechanisms deriving from the results obtained for the NO + CO and CO + O_2 reactions.

Acknowledgments

We acknowledge the financial support of the European Union's 7th Framework Programme under grant agreement No 280890-NEXT-GEN-CAT.

Appendix A. Supplementary data

Supplementary data associated with this article can be found, in the online version, at http://dx.doi.org/10.1016/j.apcatb.2015.06.017

References

[1] W.F. Libby, Science 171 (1971) 499–500.
[2] S.C. Sorenson, J.A. Wronkiewicz, L.B. Sis, G.P. Wirtz, Bull. Am. Ceram. Soc. 53 (1974) 446–449.
[3] L. Lisi, G. Bagnasco, P. Ciambelli, S. De Rossi, P. Porta, G. Russo, M. Turco, J. Solid State Chem. 146 (1999) 176–183.
[4] L. Simonot, F. Garin, G. Maire, Appl. Catal. B 11 (1997) 167–179.
[5] B. Seyfi, M. Baghalha, H. Kazemian, Chem. Eng. J. 148 (2009) 306–311.
[6] S. Cimino, G. Landi, L. Lisi, G. Russo, Catal. Today 117 (2006) 454–461.
[7] N. Guilhaume, M.J. Primet, Catalysis 165 (1997) 197–204.
[8] P. Doggali, S. Kusaba, Y. Teraoka, P. Chankapure, S. Rayalu, N. Labhsetwar, Catal. Commun. 11 (2010) 665–669.
[9] A.K. Sharma, J. Sci. Ind. Res. 63 (2004) 614–617.
[10] D. Ferri, L. Forni, Appl. Catal. B 16 (1998) 119–126.
[11] K.S. Song, H.X. Cui, S.D. Kim, S.K. Kang, Catal. Today 47 (1999) 155–160.
[12] T. Nitadori, S. Kurihara, M. Misono, J. Catal. 98 (1986) 221–228.
[13] S. Rajadurai, J.J. Carberry, B. Li, C.B. Alcock, J. Catal. 131 (1991) 582–589.
[14] N.M. Panich, G.N. Pirogova, R.I. Korosteleva, Y.V. Voronin, Russ. Chem. Bull. 48 (1999) 694–697.
[15] T. Hirano, H. Purwanto, T. Watanabe, T. Akiyama, J. Alloys Compd. 441 (2007) 263–266.
[16] Y.N. Lee, R.M. Lago, J.L.G. Fierro, V. Cortés, F. Sapiña, E. Martinez, Appl. Catal. A 207 (2001) 17–24.
[17] R. Doshi, C.B. Alcock, J.J. Carberry, Catal. Lett. 18 (1993) 337–343.
[18] A.K. Ladavos, P.J. Pomonis, Appl. Catal. B 2 (1993) 27–47.
[19] S.T. Shen, H.S. Weng, Ind. Eng. Chem. Res. 37 (1998) 2654–2661.
[20] A. Lindstedt, D. Strömberg, M. Abul Milh, Appl. Catal. A 116 (1994) 109–126.
[21] X. Wu, L. Xu, B. Yang, D. Weng, Surf. Coat. Technol. 184 (2004) 40–46.
[22] L. Forni, C. Oliva, T. Barzetti, E. Selli, A.M. Ezerets, A.V. Vishniakov, Appl. Catal. B 13 (1997) 35–43.
[23] N. Mizuno, M. Tanaka, M.J. Misono, J. Chem. Soc. Faraday Trans. 88 (1992) 91–95.
[24] X. Wu, L. Xu, D. Weng, Catal. Today 90 (2004) 199–206.
[25] L. Simonot, F. Garin, G. Maire, Appl. Catal. B 11 (1997) 181–191.
[26] V.C. Belessi, P.N. Trikalitis, A.K. Ladavos, T.V. Bakas, P.J. Pomonis, Appl. Catal. A 177 (1999) 53–58.
[27] P. Porta, S.D. Rossi, M. Faticanti, G. Minelli, I. Pettiti, L. Lisi, M. Turco, J. Solid State Chem. 146 (1999) 291–304.
[28] N. Tien-Thao, H. Alamdari, M.H. Zahedi-Niaki, S. Kaliaguine, Appl. Catal. A: Gen. 311 (2006) 204–212.
[29] N. Tien Thao, H. Alamdari, S. Kaliaguine, J. Solid State Chem. 181 (2008) 2006–2019.
[30] L. Huang, M. Bassir, S. Kaliaguine, Appl. Surf. Sci. 243 (2005) 360–375.
[31] R. Zhang, A. Villanueva, H. Alamdari, S. Kaliaguine, J. Mol. Catal. A 258 (2006) 22–34.
[32] R. Zhang, A. Villanueva, H. Alamdari, S. Kaliaguine, Appl. Catal. B 64 (2006) 220–233.
[33] B. Seyfi, M. Baghalha, H. Kazemian, Chem. Eng. J. 148 (2009) 306–311.
[34] A.N. Petrov, A.Y. Zuev, A.I. Vylkov, D.S. Tsvetkov, J. Mater. Sci. 42 (2007) 1909–1914.
[35] L. Lisi, G. Bagnasco, P. Ciambelli, S. De Rossi, P. Porta, G. Russo, M. Turco, J. Solid State Chem. 146 (1999) 176–183.
[36] A. Glisenti, A. Galenda, M.M. Natile, Appl. Catal. A 453 (2013) 102–112.
[37] D.A. Shirley, Phys. Rev. B 5 (1972) 4709–4714.
[38] J.F. Moulder, W.F. Stickle, P.E. Sobol, K.D. Bomben, Handbook of X-ray Photoelectron Spectroscopy, in: J. Chastain (Ed.), Physical Electronics, Eden Prairie, MN, 1992.
[39] D. Briggs, J.C. Riviere, Practical Surface Analysis, in: D. Briggs, M.P. Seah (Eds.), Wiley, New York, 1983.
[40] http://www.ing.unitn.it/~luttero/maud/
[41] H.R. Wenk, S. Matthies, L. Lutterotti, Mater. Sci. Forum 157–162 (1994) 473–480.
[42] M. Ferrari, L. Lutterotti, J. Appl. Phys. 76 (1994) 7246–7255.
[43] M.M. Natile, F. Poletto, A. Galenda, A. Glisenti, T. Montini, L. De Rogatis, P. Fornasiero, Chem. Mater. 20 (2008) 2314–2327.
[44] A. Galenda, M.M. Natile, V. Krishnan, H. Bertagnolli, A. Glisenti, Chem. Mater. 19 (2007) 2796–2808.
[45] A. Galenda, M.M. Natile, L. Nodari, A. Glisenti, Appl. Catal. B 97 (2010) 307–322.
[46] M. Machova, N. Braskova, P. Ivanov, J.B. Carda, V. Kozhukharov, Appl. Surf. Sci. 119 (1997) 127–136.
[47] P.A.W. van der Heide, Surf. Interface Anal. 33 (2002) 414–425.
[48] NIST XPS. Database 20, Version 3.4 (Web Version).
[49] Y. Uwamino, T. Ishizuka, H. Yamatera, J. Electron. Spectrosc. Relat. Phenom. 34 (1984) 67–78.
[50] T.L. Barr, J. Phys. Chem. 82 (1978) 1801–1810.

[51] T. Mizokawa, A. Fujimori, H. Namatame, Y. Takeda, M. Takano, Phys. Rev. B 57 (1998) 9550–9555.
[52] M.A. Peña, J.L.G. Fierro, Chem. Rev. 101 (2001) 1981–2018.
[53] R. Lago, G. Bini, M.A. Pena, J.L.G. Fierro, J. Catal. 167 (1997) 198–209.
[54] J.L.G. Fierro, Catal. Today 8 (1990) 153–174.
[55] L. Bedel, A.C. Roger, C. Estournes, A. Kiennemann, Catal. Today 85 (2003) 207–218.
[56] L.B. Sis, G.P. Wirtz, S.C. Sorenson, J. Appl. Phys. 44 (1973) 5553–5559.
[57] B. Echchahed, S. Kaliaguine, H.S. Alamdari, Int. J. Chem. React. Eng. 4 (2006) A29.
[58] H. Deng, L. Lin, S. Liu, Energy Fuels 24 (2010) 4797–4802.
[59] F. Patcas, F.C. Buciuman, J. Zsako, Therm. Acta 360 (2000) 71–76.
[60] G. Centi, S. Perathoner, L. Dall'Olio, Appl. Catal. B 7 (1996) 359–377.
[61] E.M. Sadovskaya, A.P. Suknev, L.G. Pinaeva, V.B. Goncharov, B.S. Bal'zhinimaev, C. Chupin, C. Mirodatos, J. Catal. 201 (2001) 159–168.
[62] E.M. Sadovskaya, A.P. Suknev, L.G. Pinaeva, V.B. Goncharov, B.S. Bal'zhinimaev, C. Chupin, J. Pérez-Ramírez, C. Mirodatos, J. Catal. 225 (2004) 179–189.
[63] J.M.D. Tascón, L.G. Tejuca, C.H. Rochester, J. Catal. 95 (1985) 558–566.
[64] C. Chupin, A.C. van Veen, M. Konduru, J. Després, C. Mirodatos, J. Catal. 241 (2006) 103–114.
[65] G. Centi, S. Perathoner, Appl. Catal. A: Gen. 132 (1995) 179–259.
[66] C. Zhou, X. Liu, C. Wu, Y. Wen, Y. Xue, R. Chen, Z. Zhang, B. Shan, H. Yin, W. Guo Wang, Phys. Chem. Chem. Phys. 16 (2014) 5106–5112.
[67] X.L. Xu, E. Yang, J.Q. Li, Y. Li, W.K. Chen, ChemCatChem 1 (2009) 384–392.
[68] J. Jonsson, J. Catal. 194 (2000) 55–60.
[69] P. Broqvist, I. Panas, H. Persson, J. Catal. 210 (2002) 198–206.
[70] Y. Xie, F. Dong, S. Heinbuch, J.J. Rocca, E.R. Berenstein, Phys. Chem. Chem. Phys. 12 (2010) 947–959.
[71] M.M. Natile, E. Ugel, C. Maccato, A. Glisenti, Appl. Catal. B 72 (2007) 351–362.
[72] G. Centi, S. Perathoner, Catal. Today 29 (1996) 117–122.